

## Transport Dynamics of Water Molecules Confined between Lipid Membranes

Minho Lee, Euihyun Lee, Ji-Hyun Kim, Hyonseok Hwang, Minhaeng Cho,\* and Jaeyoung Sung\*



Cite This: *J. Phys. Chem. Lett.* 2024, 15, 4437–4443



Read Online

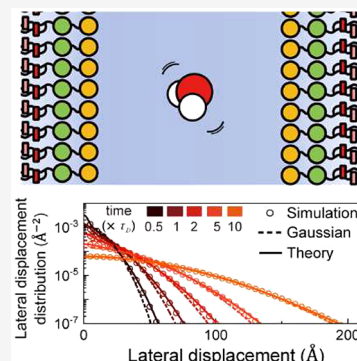
ACCESS |

Metrics & More

Article Recommendations

Supporting Information

**ABSTRACT:** Water molecules confined between biological membranes exhibit a distinctive non-Gaussian displacement distribution, far different from that of bulk water. Here, we introduce a new transport equation for water molecules in the intermembrane space, quantitatively explaining molecular dynamics simulation results. We find that the unique transport dynamics of water molecules stems from the lateral diffusion coefficient fluctuation caused by their longitudinal motion in the direction perpendicular to the membranes. We also identify an interfacial region where water possesses distinct physical properties, which is unaffected by changes in the intermembrane separation.



Water confined in biological nanospaces, such as the intermembrane regions of mitochondria, synaptic clefts, and endoplasmic reticula, is a crucial element for cell function.<sup>1–3</sup> Extensive research has investigated the structure and dynamics of water molecules in the vicinity of phosphatidylcholine (PC) bilayers, which are a major component of biological membranes. These works employed various methods including IR pump–probe spectroscopy,<sup>4–6</sup> heterodyne-detected vibration sum frequency generation (HD-VSFG),<sup>7,8</sup> nuclear magnetic resonance (NMR),<sup>9</sup> microfluidics,<sup>10–12</sup> and molecular dynamics (MD) simulation.<sup>13–21</sup> It is now established that the motility of nanoconfined water increases with its distance from the membrane center, with which the major functional groups of PC phospholipids interacting with water molecules change.<sup>4,9,14,17,18</sup> Moreover, it has been observed that dynamic motility fluctuations lead to Fickian-yet-non-Gaussian diffusion in complex fluids.<sup>22</sup> Despite these studies, however, a quantitative understanding of the time-dependent displacement distribution of nanoconfined water molecules has not yet been achieved.

To address this issue, we introduce a transport equation describing the thermal motion of molecules confined between two planar surfaces. Using MD simulations, we investigate the time-dependent displacement distribution of water molecules nanoconfined between two lipid membranes composed of 1,2-dimyristoyl-sn-glycero-3-phosphocholine (DMPC) lipids. The solution derived from our transport equation provides a quantitative explanation of the MD simulation results for the mean square displacement, the non-Gaussian parameter, and the displacement distribution. Our analysis shows that nanoconfined water exhibits a super-Gaussian lateral displace-

ment distribution originating from dynamic fluctuations of the lateral diffusion coefficient due to its coupling to water motion in the longitudinal direction. The time-dependent deviation of this lateral displacement distribution from Gaussian is found to be strongly influenced by the intermembrane separation. We also identify an interfacial region where water molecules have structures and dynamics that are distinct from bulk water and robust with respect to changes in intermembrane separation.

The essential assumption underlying our transport equation is that the most important variable that affects the lateral thermal motion of an interfacial water molecule is the distance,  $z$ , between the water molecule and the center of the membrane. This is a legitimate assumption because the microscopic environment interacting with a water molecule, including the functional groups of lipid molecules and hydrogen bond network, drastically changes with  $z$ .<sup>9,17,18</sup> Under this assumption, we obtain the following transport equation governing transport dynamics of interfacial water, starting from a general model of thermal motion coupled to environmental variables:<sup>23</sup>

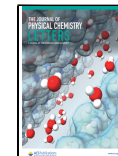
$$\hat{p}(\mathbf{r}_{||}, z, s) = \hat{\mathcal{D}}_{||}(z, s) \nabla_{||}^2 \hat{p}(\mathbf{r}_{||}, z, s) + L(z) \hat{p}(\mathbf{r}_{||}, z, s) \quad (1)$$

Received: February 1, 2024

Revised: March 23, 2024

Accepted: March 26, 2024

Published: April 16, 2024



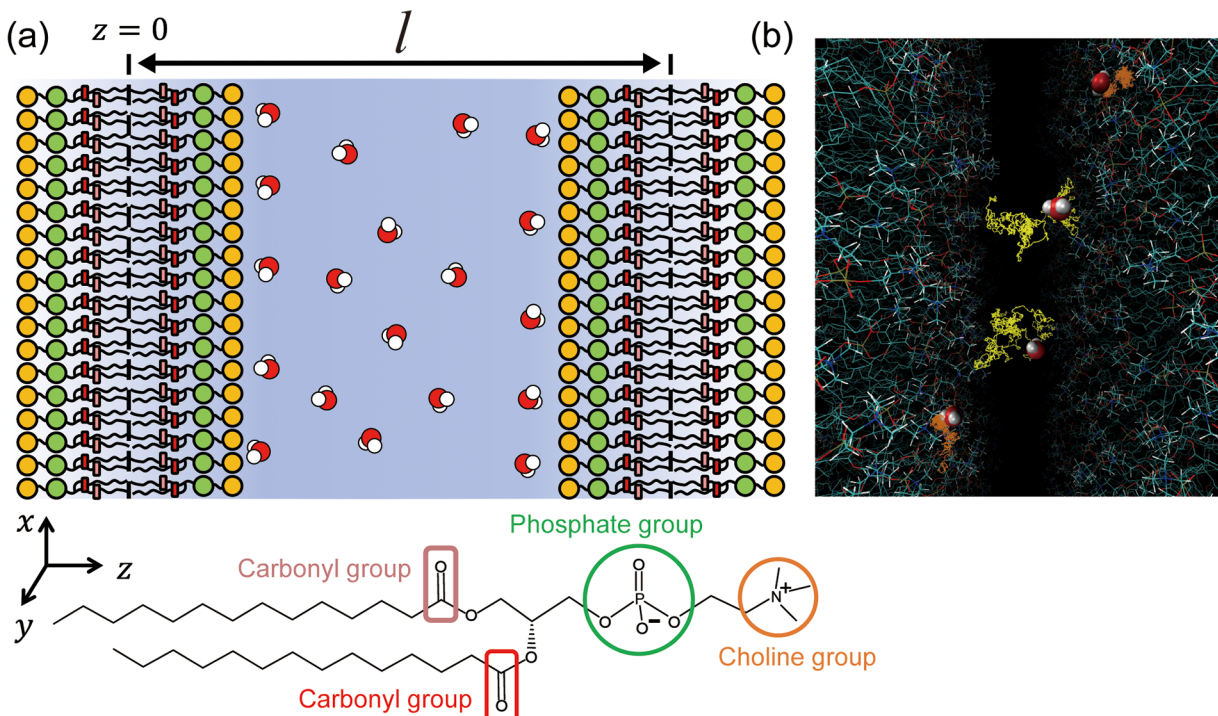


**Figure 1.** (a) Schematic representation of our MD simulation system: water molecules confined between two DMPC lipid bilayers. The simulation was performed for the system with three different intermembrane separations, i.e.,  $l = 53.2 \text{ \AA}$ ,  $61.8 \text{ \AA}$ , and  $80.6 \text{ \AA}$ . (b) Representative trajectories of water molecules undergoing thermal motion between the lipid bilayers for  $50 \text{ ps}$ : (yellow lines) the trajectories of water molecules freely moving near the center of the intermembrane space; (orange lines) trajectories of water molecules strongly interacting with the lipid head groups of DMPC.

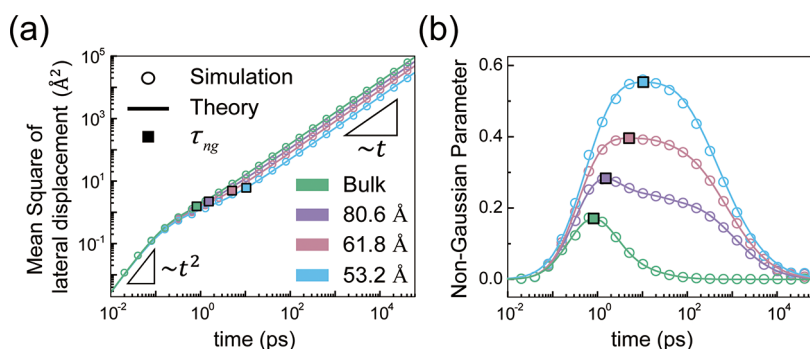


**Figure 2.** (a) Mean square displacement (MSD) and (b) non-Gaussian parameter (NGP) associated with the lateral displacement of water molecules for systems with various intermembrane separations: (circles) simulation results (solid lines) eq S19 for MSD and eq S21 for NGP (square) the NGP peak time ( $\tau_{ng}$ ).

where  $\hat{p}(\mathbf{r}_{\parallel}, z, s)$  denotes the Laplace transform of the joint probability density,  $p(\mathbf{r}_{\parallel}, z, t)$ , that a water molecule is located at lateral position  $\mathbf{r}_{\parallel}$  ( $= (x, y)$ ) and the distance between the water molecule and the center of the membrane is  $z$  at time  $t$ .  $\hat{f}(s)$  and  $\hat{f}'(s)$  denote the Laplace transform of  $f(t)$  and  $\partial_t f(t)$ , i.e.,  $\hat{f}(s) = \int_0^\infty dt e^{-st} f(t)$  and  $\hat{f}'(s) = \int_0^\infty dt e^{-st} \partial_t f(t)$ .  $\nabla_{\parallel}^2$  denotes the Laplacian in the two-dimensional space parallel to the lipid membrane. In eq 1,  $\hat{\mathcal{D}}_{\parallel}(z, s)$  represents the lateral diffusion kernel dependent on  $z$ . Its small- $s$  limit,  $\hat{\mathcal{D}}_{\parallel}(z, 0)$ , serves as the lateral diffusion coefficient,  $D_{\parallel}(z)$ , of water molecules separated by  $z$  from the center of the membrane. In eq 1,  $L(z)$  denotes a mathematical operator describing the transport dynamics of the water molecules in a direction perpendicular to the membrane surface.

We then investigate the mean square displacement (MSD),  $\Delta_2(t)$ , and non-Gaussian parameters (NGP),  $\alpha_2(t)$  [ $\equiv \Delta_4(t)/(2\Delta_2(t)^2) - 1$ ], of the lateral displacement distribution of the water molecules. Here,  $\Delta_2(t)$  and  $\Delta_4(t)$  denote the second and fourth moments of the time-dependent distribution of the water displacement,  $\Delta\mathbf{r}_{\parallel}(t)[\equiv \mathbf{r}_{\parallel}(t) - \mathbf{r}_{\parallel}(0)]$ , in the lateral direction. The NGP vanishes when the displacement distribution is Gaussian.<sup>24,25</sup> From eq 1, analytic expressions of the  $\Delta_2(t)$  and  $\Delta_4(t)$  can be obtained as

$$\hat{\Delta}_2(s) = \frac{4}{s^2} \langle \hat{\mathcal{D}}_{\parallel}(s) \rangle \quad (2a)$$

$$\hat{\Delta}_4(s) = 4s\hat{\Delta}_2(s)^2 [1 + s\hat{C}_{\mathcal{D}}(s)] \quad (2b)$$

In eq 2a,  $\langle \mathcal{D}_{\parallel}(t) \rangle$  denotes the mean diffusion kernel of water molecules.  $\langle Q \rangle$  designates the average of quantity  $Q(z)$  over the equilibrium distribution,  $P_{eq}(z)$ , of  $z$ .  $\langle \mathcal{D}_{\parallel}(t) \rangle$  is the same as the lateral velocity autocorrelation function (VAF) of water molecules divided by 2.<sup>23</sup> In eq 2b,  $C_{\mathcal{D}}(t)$  denotes the lateral diffusion kernel correlation (DKC) defined by

$$\begin{aligned} \hat{C}_{\mathcal{D}}(s) &= \int_0^l dz \int_0^l dz_0 \frac{\delta \hat{\mathcal{D}}_{\parallel}(z, s)}{\langle \hat{\mathcal{D}}_{\parallel}(s) \rangle} \hat{G}(z, slz_0) \\ &\times \frac{\delta \hat{\mathcal{D}}_{\parallel}(z_0, s)}{\langle \hat{\mathcal{D}}_{\parallel}(s) \rangle} P_{eq}(z_0) \end{aligned} \quad (3)$$

where 0 and  $l$  denote the center positions of the two membranes confining water molecules (see Figure 1). In eq 3,  $\delta \hat{\mathcal{D}}_{\parallel}(z, s)$  and  $G(z, tlz_0)$  denote, respectively,  $\hat{\mathcal{D}}_{\parallel}(z, s) - \langle \hat{\mathcal{D}}_{\parallel}(s) \rangle$  and the Green's function, or the conditional probability that a water molecule initially located at  $z_0$  is found at  $z$  at time  $t$ , defined by  $\partial_t G(z, tlz_0) = L(z)G(z, tlz_0)$  with the initial condition,  $G(z, 0|z_0) = \delta(z - z_0)$ . Equation 2a enables us to extract the time profile of the DKC from the MSD and the NGP or the first two nonvanishing moments of the displacement distribution (see Figure S3a in the Supporting Information).

At the onset of Fickian diffusion, the NGP reached its maximum value (Figure 2). Beyond this NGP peak time, the MSD of water molecules linearly increases with time, which results because the VAF or  $\langle \mathcal{D}_{\parallel}(t) \rangle$  is negligibly small after the NGP peak time, i.e.,  $\Delta_2(t) = 4 \int_0^t d\tau (t - \tau) \langle \mathcal{D}_{\parallel}(\tau) \rangle \cong 4t \int_0^\infty \langle \mathcal{D}_{\parallel}(\tau) \rangle$ . At time scales longer than the NGP peak time,  $L(z)$  in eq 1 can be approximated by the following Smoluchowski operator, i.e.,  $L(z) \cong L_{SM}(z) = \partial_z [D_{\perp}(z) (\partial_z + \beta U(z))]$ . Here,  $D_{\perp}(z)$  and  $\beta U(z)$ , respectively, denote the  $z$ -dependent diffusion coefficient associated with the thermal motion of water molecules in the direction perpendicular to the membrane and the thermal energy-scaled potential of mean force with  $\beta = 1/k_B T$ .  $k_B$  and  $T$  denote the Boltzmann constant and temperature, respectively. After the onset of Fickian diffusion, the MSD and NGP of the lateral diffusion of water molecules assume the following analytic forms:

$$\Delta_2(t) \cong 4 \langle D_{\parallel} \rangle t \quad (4a)$$

$$\alpha_2(t) \cong \frac{2\eta_D^2}{t^2} \int_0^t dt' (t - t') \phi_D(t') \quad (4b)$$

In eq 4,  $\langle D_{\parallel} \rangle$  and  $\eta_D^2 [= \langle \delta D_{\parallel}^2 \rangle / \langle D_{\parallel} \rangle^2]$  denote, respectively, the mean diffusion coefficient defined by  $\langle D_{\parallel} \rangle = \int_0^\infty \langle \mathcal{D}_{\parallel}(\tau) \rangle$  and the relative variance of the  $z$ -dependent lateral diffusion coefficient, with  $\delta f$  denoting the deviation of a quantity  $f$  from its mean, i.e.,  $\delta f(z) = f(z) - \langle f \rangle$ .  $\phi_D(t)$  denotes the normalized time-correlation function (TCF) of the lateral diffusion coefficient fluctuation, i.e.,

$$\begin{aligned} \phi_D(t) &= \frac{\langle \delta D_{\parallel}(t) \delta D_{\parallel}(0) \rangle}{\langle \delta D_{\parallel}^2 \rangle} \\ &= \langle \delta D_{\parallel}^2 \rangle^{-1} \int_0^l dz \int_0^l dz_0 \delta D_{\parallel}(z) G_{SM}(z, tlz_0) \delta D_{\parallel}(z_0) P_{eq}(z_0) \end{aligned} \quad (5)$$

where  $G_{SM}(z, tlz_0)$  designates Green's function of Smoluchowski equation governing the thermal motion of water molecules in the direction perpendicular to the membranes, i.e.,  $\partial_t G_{SM}(z, tlz_0) = L_{SM}(z)G_{SM}(z, tlz_0)$ , with the initial condition,  $G_{SM}(z, 0|z_0) = \delta(z - z_0)$ .

Equations 4b and 5 indicate that, for nanoconfined water molecules, the non-Gaussian diffusion in the lateral direction originates from the fluctuation of the lateral diffusion coefficient coupled to water motion in the longitudinal direction. We note here that the DKC defined in eq 3 reduces to  $\eta_D^2 \phi_D(t)$  at long times where the MSD linearly increases with time; the long-time profile of  $C_{\mathcal{D}}(t)$  extracted from the MSD and NGP time profiles of our MD simulation results is in quantitative agreement with our theoretical result for  $\eta_D^2 \phi_D(t)$  calculated using eq 5. This agreement between simulation and theory supports the validity of our assumption underlying eq 1 that the dynamic fluctuation in the lateral diffusion coefficient of water molecules primarily originates from its coupling to the thermal motion of water molecules in the longitudinal direction.

We also performed MD simulation study on the thermal motion of water molecules in the intermembrane space, for a system of SPC/E water molecules confined between two lipid bilayers, each composed of 128 DMPC molecules, systematically changing the ratio of the number of water molecules to the number of lipid molecules and the distance  $l$  between the two membrane centers (Figure 1). We employed the AMBER lipid 14 force field for simulation of the lipid molecules<sup>26</sup> and imposed periodic boundary conditions on the system. We also investigated the transport dynamics of a pure, bulk water system, using the MD simulation of 5000 SPC/E water molecules and compared it to the transport dynamics of the nanoconfined water molecules. Our MD simulation was conducted for a system at a temperature of 318 K in the NVT ensemble. Additional information about the simulations can be found in the Supporting Information.

From the MD simulation trajectories of water molecules, we obtained the MSD and NGP of the lateral water displacement for each system (Figure 2). The time profile of the MSD obtained from the MD simulation exhibits a dynamic transition behavior that is dependent on the separation between the two lipid membranes (Figure 2a). The time profile of the MSD shows the transition from an initial ballistic motion ( $\Delta_2(t) \sim t^2$ ) to terminal Fickian diffusion ( $\Delta_2(t) \sim t^1$ ), with intermediate subdiffusion ( $\Delta_2(t) \sim t^\alpha$  with  $0 < \alpha < 1$ ). The short-time ballistic behavior of the MSD shows little variation with changes in  $l$  and quadratically increases with time, i.e.,  $\Delta_2(t) = 2k_B T t^2 / M$ .<sup>23</sup> Here,  $M$  denotes the mass of a water molecule. However, the intermediate subdiffusive regime becomes more pronounced, and the value of long-time lateral diffusion coefficient gets smaller as the separation,  $l$ , between lipid bilayers decreases. These findings align with previous studies.<sup>10,12,16,21</sup> The time profiles of the MSD could be quantitatively explained by using the analytic formula for the MSD of a bead in a Gaussian polymer (see Figure 2a), which is decomposable into an unbound-mode and multiple bound-

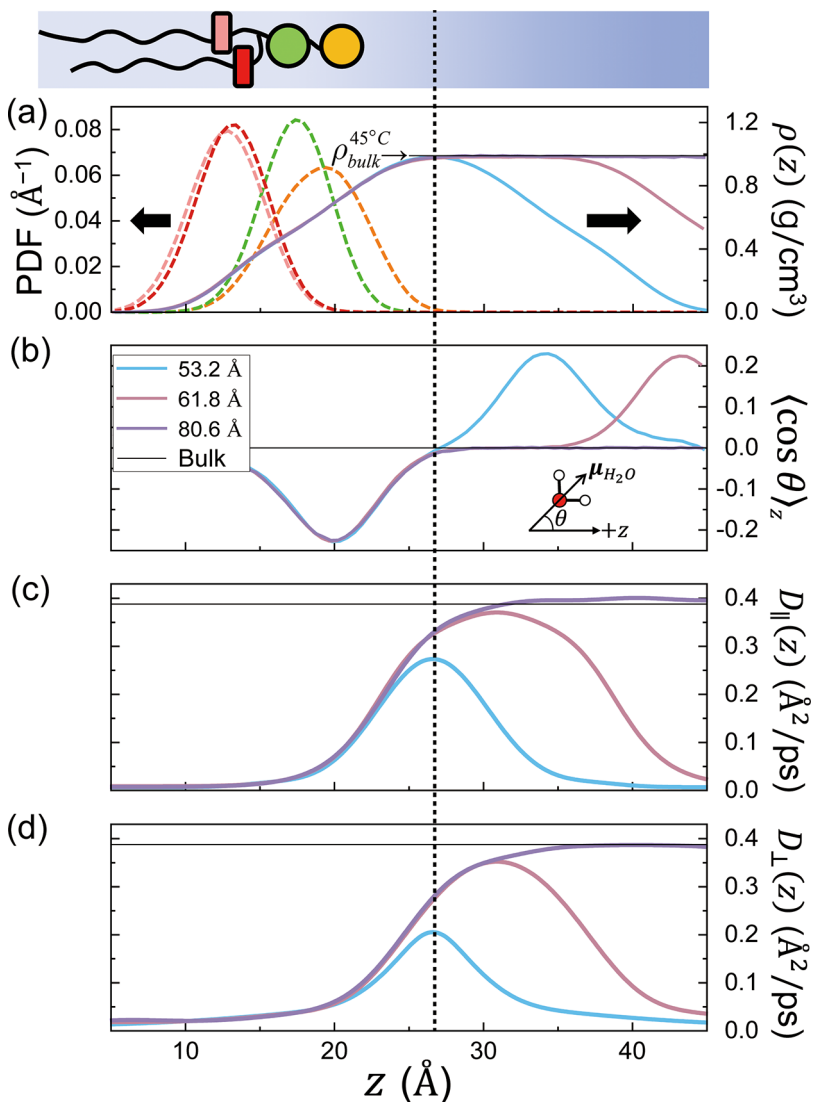


**Figure 3.** Dependence of structural and dynamical properties of the water molecules on the distance  $z$  from the center of the lipid membrane in the left.  $z$ -dependent profile of (a) mass density,  $\rho(z)$ , (b) orientation  $\langle \cos \theta \rangle_z$ , (c) lateral diffusion coefficient,  $D_{\parallel}(z)$ , and (d) longitudinal diffusion coefficient,  $D_{\perp}(z)$ , of water molecules.  $\theta$  designates the angle between the water moment and the longitudinal axis. (dotted line) the position of the boundary,  $z_c = 26.6$  Å, between interfacial water region and bulk-like water region. (dashed lines) probability distribution of the positions of various functional groups in the DMPC: (orange) the nitrogen atom in the choline group (green) phosphorus atom in the phosphate group (red and pink) the oxygen atoms in the two carbonyl groups. The probability distribution of these functional groups as well as the  $z$ -dependent profiles of  $\rho(z)$  and  $\langle \cos \theta \rangle_z$  are largely independent of the intermembrane separation.

mode terms.<sup>23</sup> For bulk water at room temperature, the bound-mode terms, which cause intermediate subdiffusion, are negligible. However, for intermembrane water, the contribution from bound-modes increases as the separation,  $l$ , between the membranes decreases. This indicates that the bound mode terms result from interfacial water molecules, which are transiently trapped by lipid membranes.

Our MD simulation study reveals that both the NGP peak time and the peak height increase as the separation,  $l$ , between the membranes decreases (Figure 2b). A longer peak time and a greater peak height of the NGP signify, respectively, prolonged trapping of water molecules<sup>23,27</sup> and increased fluctuation in the lateral diffusion coefficient (see eq 4b). These phenomena can be attributed to the attractive interactions between interfacial water molecules and the functional groups in the lipid molecules. As  $l$  decreases, the proportion of the trapped interfacial water molecules grows,

leading to a decrease in the mean lateral diffusion coefficient and an increase in the variance of the diffusion coefficient.

At times longer than the NGP peak time, the nanoconfined molecules undergo Fickian-yet-non-Gaussian diffusion, with the NGP value decreasing with time. The nanoconfined water molecules have a NGP value far greater than that of bulk water molecules. The NGP of bulk water molecules becomes negligible at times longer than 10 ps; in contrast, the NGP of the nanoconfined water molecules does not vanish at times longer than 10 ns. The NGP shows a strongly nonexponential relaxation dynamics, whose time profile can be quantitatively explained by eqs 4b and 5 as shown later in this Letter.

We then identify the interfacial region where water molecules directly interact with the lipid head groups. For this purpose, we investigate the structure and dynamics of water molecules near the lipid bilayers using the MD simulations. Figure 3a and 3b show the  $z$ -dependence of the

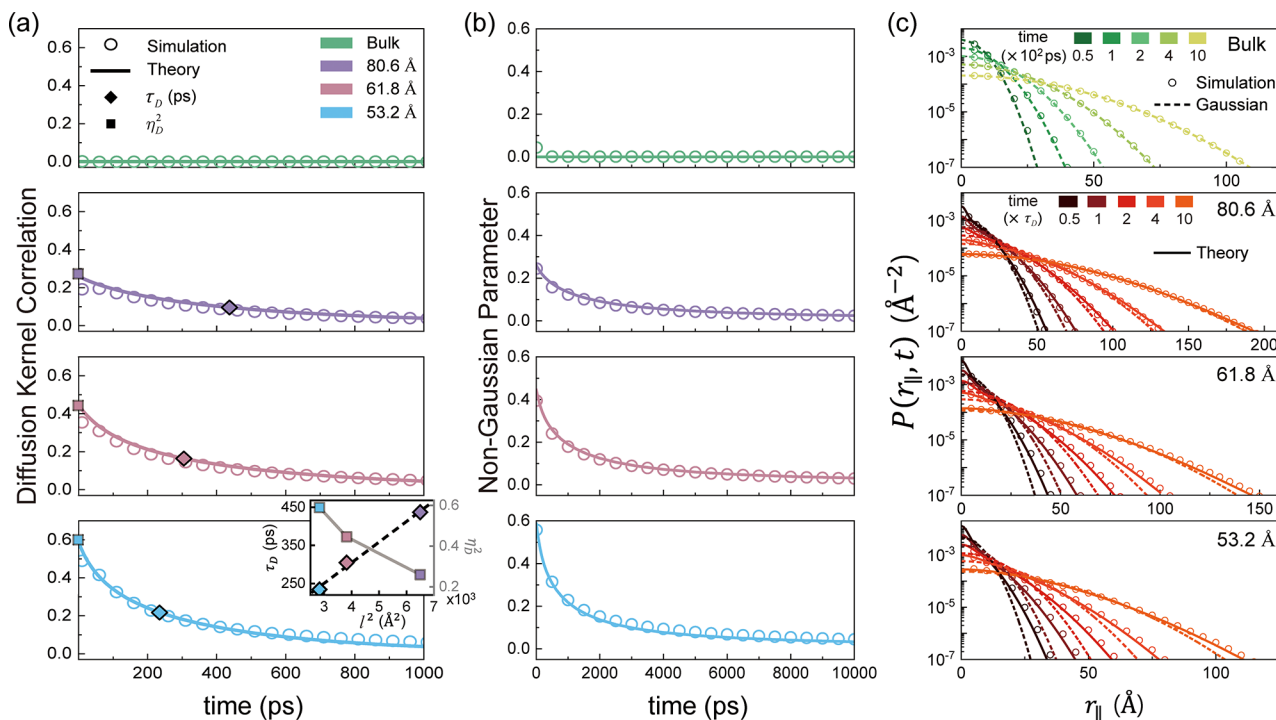


**Figure 4.** Diffusion kernel correlation, non-Gaussian parameter, and lateral displacement distribution of water molecules confined between two lipid membranes with various intermembrane separations. (a) Comparison between the diffusion kernel correlation and the mean-scaled time correlation function of the lateral diffusion coefficient fluctuation: (circles) diffusion kernel correlation,  $C_D(t)$ , from the MD simulation results; (solid lines) mean-scaled TCFs,  $\eta_D^2\phi_D(t)$ , of the lateral diffusion coefficient fluctuation calculated by eq 5; (diamond) relaxation time  $\tau_D$  defined by  $\phi_D(\tau_D) = e^{-1}$ ; (square) the value of the relative variance,  $\eta_D^2$ , of the diffusion coefficient. (Inset in (a)) Dependence of  $\tau_D$  and  $\eta_D^2$  on the square,  $l^2$ , of intermembrane separation. (b) Non-Gaussian parameter  $\alpha_2(t)$ : (circles) simulation; (solid line) eq 4b. (c) Lateral displacement distributions at various times: (circles) simulation results; (solid lines) theoretical predictions; (dotted line) Gaussian with zero mean and variance given by  $4\langle D_{||} \rangle t$ .

density profile,  $\rho(z)$ , and the dipole orientation profile,  $\langle \cos \theta \rangle_z$ , of the nanoconfined water. Here,  $\theta$  and bracket  $\langle \dots \rangle_z$  denote the angle between the water dipole moment and the  $z$ -axis and the average over water molecules located within an interval ( $z - 0.25 \text{ \AA}$ ,  $z + 0.25 \text{ \AA}$ ), respectively. As shown in Figure 3a, the water molecules in close vicinity of the membrane exhibit a lower density compared to the density,  $\rho_{\text{bulk}}^{45^\circ\text{C}} = 0.99 \text{ g cm}^{-3}$ , of bulk water.<sup>28</sup> The dipole orientation profile,  $\langle \cos \theta \rangle_z$ , does not vanish for water molecules in the vicinity of the functional groups in the lipid molecules. This results from the nonisotropic interactions between the water molecules and those functional groups, whose positions along the  $z$ -direction are shown in Figure 3a. At positions near  $z \approx 20 \text{ \AA}$ ,  $\langle \cos \theta \rangle_z$  has a negative value, while at positions near  $z \approx l - 20 \text{ \AA}$ , it has a positive value, indicating that the water dipole moment tends to point toward phosphate and carbonyl groups rather than choline groups.<sup>7,8</sup> This is because water molecules in the vicinity of phosphate and carbonyl groups experience strong restrictions on their orientations due to the hydrogen bonding with these groups, whereas those near choline groups exhibit broadly distributed angle distribution, forming the clathrate-like hydration shell around the choline groups.<sup>4,13</sup>

Remarkably, the density and dipole orientation profiles show little dependence on  $l$  for the interfacial water molecules at  $z$  smaller than  $z_c = 26.6 \text{ \AA}$  but recover their respective bulk-limit values in the intermediate region defined by  $z_c \leq z \leq l - z_c$ . Based on these observations, we define  $z_c$  as the boundary between the interfacial water region and the bulk-like water region. The value of  $z_c$  ( $= 26.6 \text{ \AA}$ ) estimated from our MD simulation is found to be comparable to the previously

reported  $z_c$  values, 24 and 28  $\text{\AA}$ , which were estimated by investigating the structural order<sup>15</sup> and the rotational dynamics<sup>19</sup> of water molecules near the lipid membrane.

The diffusion coefficients of water molecules are also strongly dependent on their distances from the membrane. We obtain the  $z$ -dependent profiles of  $D_{||}(z)$  and  $D_{\perp}(z)$  (Figure 3c,d) using umbrella sampling and mean first passage time analysis (Figures S1 and S2), respectively.<sup>14,29</sup> Within the interfacial water region ( $z < z_c$ ), both the diffusion coefficients increase with  $z$ , and their  $z$ -dependent profiles are also similar across various intermembrane separations. For the system with  $l = 80.6 \text{ \AA}$ , both diffusion coefficients recover the bulk-limit value,  $D_{\text{bulk}}^{45^\circ\text{C}} = 3.88 \times 10^{-1} \text{ \AA}^2 \cdot \text{ps}^{-1}$ , of the SPC/E water at distances greater than  $z_c$ . However, for the systems with  $l < 80.6 \text{ \AA}$ , the values of  $D_{||}(z)$  and  $D_{\perp}(z)$  are smaller than  $D_{\text{bulk}}^{45^\circ\text{C}}$  across the entire  $z$  region. For example, when the value of  $l$  is 53.2  $\text{\AA}$ , the maximum values of  $D_{||}(l/2)$  and  $D_{\perp}(l/2)$  are only about 70% and 50% of  $D_{\text{bulk}}^{45^\circ\text{C}}$ , respectively. Noting that the longitudinal position,  $z$ , of the central nitrogen atom in the choline group is about  $19.3 \pm 4 \text{ \AA}$  (Figure 3a), these results suggest that the choline group in the lipid molecule retard the translational motion of water molecules located beyond its first hydration shell, which extends about 4.5  $\text{\AA}$  from the central nitrogen atom in the choline group.<sup>13</sup>

The  $z$ -dependence profiles of water density  $\rho(z)$  and the diffusion coefficients,  $D_{||}(z)$  and  $D_{\perp}(z)$ , are related to the time profile of  $\eta_D^2\phi_D(t)$  and the NGP according to eqs 4b and 5. Equation 4b tells us that, after the onset of Fickian diffusion, the NGP time profile is completely determined by the mean-

scaled TCF,  $\eta_D^2 \phi_D(t) [= \langle \delta D_{||}(t) \delta D_{||}(0) \rangle / \langle D_{||} \rangle^2]$ , of the diffusion coefficient fluctuation. Here,  $\eta_D^2 [= \langle D_{||}^2 \rangle / \langle D_{||} \rangle^2 - 1]$  can be calculated from  $D_{||}(z)$  and  $\rho(z)$  by using  $\langle D_{||}^n \rangle = \int_0^l dz D_{||}^n(z) P_{eq}(z)$  with  $P_{eq}(z) = \rho(z) / \int_0^l dz \rho(z)$ .  $\phi_D(t)$  can also be calculated from eq 5, where the Green's function  $G_{SM}(z, tlz_0)$  is obtained by solving  $\partial_t G_{SM}(z, tlz_0) = \partial_z [D_{\perp}(z) (\partial_z + \partial_{tlz_0}) \beta U(z)] G_{SM}(z, tlz_0)$  with the initial condition  $G_{SM}(z, 0lz_0) = \delta(z - z_0)$ . The thermal energy-scaled potential of mean force,  $\beta U(z)$ , can be estimated from  $\rho(z)$  by  $\beta U(z) = -\ln[\rho(z)/\rho_{bulk}^{45^\circ C}]$ . Across systems with various intermembrane separations, the result of  $\eta_D^2 \phi_D(t)$  calculated using our theory closely matches the long-time profile of  $C_D(t)$  directly extracted from the MD simulation results (Figure 4a). In addition, the NGP time profiles calculated from eq 4b are also in quantitative agreement with the MD simulation results (Figure 4b). Furthermore, our theory predicts the lateral displacement distribution with a unimodal peak and a non-Gaussian tail for nanoconfined water molecules. We find the prediction of our theory to be in excellent agreement with the MD simulation results for the time-dependent lateral displacement distribution of water molecules at various times and separations between the membranes (Figure 4c). The agreement between theory and simulation again demonstrates the validity of our assumption underlying eq 1, that is, the most important variable that affects the lateral thermal motion of an interfacial water molecule is the distance,  $z$ , between a water molecule and the center of the membrane.

The relaxation time  $\tau_D$  of  $\phi_D(t)$ , defined by  $\phi_D(\tau_D) = e^{-1}$ , quadratically increases with the intermembrane separation  $l$  (see inset of Figure 4a). This follows because, for the complete relaxation of the diffusion coefficient fluctuation, water molecules must travel the entire intermembrane space, and the time taken for this process should be proportional to the mean first passage time, which quadratically increases with  $l$  (see Movie S1 in the Supporting Information). On the other hand,  $\eta_D^2$  decreases with  $l$ . This is because, as  $l$  increases, the proportion of the trapped interfacial water molecules decreases, which leads to an increase in the mean lateral diffusion coefficient and a decrease in the variance of the diffusion coefficient.

We note here that at times shorter than 0.1 ps, the NGP increases with time, which cannot be explained by eq 4b. At such short times, the DKC can be approximated by  $C_D(t) \cong 2[\langle D_{||}(t) \rangle / \langle D_{||}(0) \rangle]^2 = 2\phi_v^2(t)$  (see Figure S3a in the Supporting Information), where  $\phi_v(t)$  denotes the normalized VAF of water molecules. Using this approximation in eq 2b, we obtained the following short-time asymptotic expression of the NGP as

$$\alpha_2(t) = \frac{1}{18}(\gamma^2 - \mu)t^2 + O(t^3) \quad (6)$$

where  $\gamma$  and  $\mu$  denote  $-\lim_{t \rightarrow 0} \partial \phi_v(t) / \partial t$  and  $\lim_{t \rightarrow 0} \partial^2 \phi_v(t) / \partial t^2$ , respectively. Explicit expressions of  $\gamma$  and  $\mu$  are available for our model (see the paragraph below eq S24 in the Supporting Information). According to this result, the NGP quadratically increases with time, which quantitatively explains our simulation results for the short-time asymptotic behavior of the NGP.

The major contributor to the short-time dynamics of the NGP is the relaxation dynamics of the velocity fluctuation, and

the two-time velocity autocorrelation function completely determines the NGP time profile. After the onset of Fickian diffusion, however, the relaxation dynamics of the diffusion coefficient fluctuation additionally contributes to the NGP time profile. For the bulk water system, where the diffusion coefficient fluctuation is negligible, the short-time asymptotic expression of the NGP that only accounts for the velocity relaxation provides a quantitative explanation of the long-time relaxation of the NGP as well as the short-time relaxation (see Figure S3b in the Supporting Information).

We present a physical model and transport equation that quantitatively explain the stochastic thermal motion of water molecules in intermembrane space. The lateral displacement distribution of the water molecules nanoconfined between two membranes strongly deviates from Gaussian, which originates from the dynamic fluctuation in the lateral diffusion coefficient. This fluctuation occurs because the lateral diffusion coefficient of a water molecule primarily depends on its distance from the membrane center, and this distance fluctuates over time owing to thermal motion of the water molecule in the longitudinal direction. In addition, using the molecular dynamics (MD) simulation, we investigate the dependence of the mass density, the orientation, and the lateral and longitudinal diffusion coefficients of a water molecule nanoconfined between two phospholipid membranes on its distance from the phospholipid membrane center. This study shows the presence of an interfacial region within 26.6 Å from the membrane center. Water molecules in the interfacial region have a structure and dynamics far different from those of bulk water molecules. The properties of interfacial water molecules are robust with respect to changes in the intermembrane separation. Our theory provides a unified, quantitative explanation of our MD simulation results for the mean square displacement, non-Gaussian parameter, and displacement distribution of nanoconfined water molecules. Our model is applicable or can be extended to quantitative investigation into the dynamics of transport and transport-coupled processes occurring in various nanoconfined environments.

## ASSOCIATED CONTENT

### Supporting Information

The Supporting Information is available free of charge at <https://pubs.acs.org/doi/10.1021/acs.jpcllett.4c00323>.

Additional figures, tables, computational details for MD simulation and captions for Movie S1 ([PDF](#))

Movie S1: Heatmap of discrete Green's function ([MP4](#))

Transparent Peer Review report available ([PDF](#))

## AUTHOR INFORMATION

### Corresponding Authors

**Jae young Sung** — Creative Research Initiative Center for Chemical Dynamics in Living Cells, Chung-Ang University, Seoul 06974, Republic of Korea; Department of Chemistry, Chung-Ang University, Seoul 06974, Republic of Korea;  [orcid.org/0000-0003-0712-296X](https://orcid.org/0000-0003-0712-296X); Email: [jaeyoung@cau.ac.kr](mailto:jaeyoung@cau.ac.kr)

**Minhaeng Cho** — Center for Molecular Spectroscopy and Dynamics, Institute for Basic Science (IBS), Seoul 02841, Republic of Korea; Department of Chemistry, Korea University, Seoul 02841, Republic of Korea;  [orcid.org/0000-0003-1618-1056](https://orcid.org/0000-0003-1618-1056); Email: [mcho@korea.ac.kr](mailto:mcho@korea.ac.kr)

**Authors**

**Minho Lee** — *Creative Research Initiative Center for Chemical Dynamics in Living Cells, Chung-Ang University, Seoul 06974, Republic of Korea; Department of Chemistry, Chung-Ang University, Seoul 06974, Republic of Korea*

**Euihyun Lee** — *Department of Chemistry, The University of Texas at Austin, Austin, Texas 78757, United States*

**Ji-Hyun Kim** — *Creative Research Initiative Center for Chemical Dynamics in Living Cells, Chung-Ang University, Seoul 06974, Republic of Korea; Department of Chemistry, Chung-Ang University, Seoul 06974, Republic of Korea*

**Hyonseok Hwang** — *Department of Chemistry, Institute for Molecular Science and Fusion Technology, Kangwon National University, Gangwon-do 24341, Republic of Korea;*  
 [orcid.org/0000-0002-7480-6723](https://orcid.org/0000-0002-7480-6723)

Complete contact information is available at:  
<https://pubs.acs.org/10.1021/acs.jpcllett.4c00323>

**Notes**

The authors declare no competing financial interest.

**ACKNOWLEDGMENTS**

This work was supported by the Institute for Basic Science (IBS-R023-D1), the Creative Research Initiative Project program (RS-2015-NR011925) funded by the National Research Foundation (NRF) of Korea, and the NRF grants (NRF-2020R1A2C1102788 and RS-2023-00245431) funded by Korea government (MSIT).

**REFERENCES**

- (1) Demirel, Y.; Gerbaud, V. *Chapter 11 - Thermodynamics and Biological Systems. In Nonequilibrium Thermodynamics*, 4th ed.; Elsevier, 2019; pp 489–571.
- (2) McCann, F. E.; Vanherberghe, B.; Eleme, K.; Carlin, L. M.; Newsam, R. J.; Goulding, D.; Davis, D. M. The Size of the Synaptic Cleft and Distinct Distributions of Filamentous Actin, Ezrin, CD43, and CD45 at Activating and Inhibitory Human NK Cell Immune Synapses. *J. Immunol.* **2003**, *170* (6), 2862–2870.
- (3) Terasaki, M.; Shemesh, T.; Kasthuri, N.; Klemm, R. W.; Schalek, R.; Hayworth, K. J.; Hand, A. R.; Yankova, M.; Huber, G.; Lichtman, J. W.; Rapoport, T. A.; Kozlov, M. M. Stacked Endoplasmic Reticulum Sheets Are Connected by Helicoidal Membrane Motifs. *Cell* **2013**, *154* (2), 285–296.
- (4) Zhao, W.; Moilanen, D. E.; Fenn, E. E.; Fayer, M. D. Water at the Surfaces of Aligned Phospholipid Multibilayer Model Membranes Probed with Ultrafast Vibrational Spectroscopy. *J. Am. Chem. Soc.* **2008**, *130* (42), 13927–13937.
- (5) Kundu, A.; Kwak, K.; Cho, M. Water Structure at the Lipid Multibilayer Surface: Anionic Versus Cationic Head Group Effects. *J. Phys. Chem. B* **2016**, *120* (22), 5002–5007.
- (6) Kundu, A.; Blasiak, B.; Lim, J.-H.; Kwak, K.; Cho, M. Water Hydrogen-Bonding Network Structure and Dynamics at Phospholipid Multibilayer Surface: Femtosecond Mid-IR Pump–Probe Spectroscopy. *J. Phys. Chem. Lett.* **2016**, *7* (5), 741–745.
- (7) Mondal, J. A.; Nihonyanagi, S.; Yamaguchi, S.; Tahara, T. Three Distinct Water Structures at a Zwitterionic Lipid/Water Interface Revealed by Heterodyne-Detected Vibrational Sum Frequency Generation. *J. Am. Chem. Soc.* **2012**, *134* (18), 7842–7850.
- (8) Dreier, L. B.; Wolde-Kidan, A.; Bonthuis, D. J.; Netz, R. R.; Backus, E. H. G.; Bonn, M. Unraveling the Origin of the Apparent Charge of Zwitterionic Lipid Layers. *J. Phys. Chem. Lett.* **2019**, *10* (20), 6355–6359.
- (9) Zhang, R.; Cross, T. A.; Peng, X.; Fu, R. Surprising Rigidity of Functionally Important Water Molecules Buried in the Lipid Headgroup Region. *J. Am. Chem. Soc.* **2022**, *144* (17), 7881–7888.
- (10) Kazoe, Y.; Mawatari, K.; Li, L.; Emon, H.; Miyawaki, N.; Chinen, H.; Morikawa, K.; Yoshizaki, A.; Dittrich, P. S.; Kitamori, T. Lipid Bilayer-Modified Nanofluidic Channels of Sizes with Hundreds of Nanometers for Characterization of Confined Water and Molecular/Ion Transport. *J. Phys. Chem. Lett.* **2020**, *11* (14), 5756–5762.
- (11) Saruko, T.; Morikawa, K.; Kitamori, T.; Mawatari, K. Proton Diffusion and Hydrolysis Enzymatic Reaction in 100 nm Scale Biomimetic Nanochannels. *Biomicrofluidics* **2022**, *16* (4), No. 044109.
- (12) Kazoe, Y.; Ikeda, K.; Mino, K.; Morikawa, K.; Mawatari, K.; Kitamori, T. Quantitative Characterization of Liquids Flowing in Geometrically Controlled Sub-100 nm Nanofluidic Channels. *Anal. Sci.* **2023**, *39*, 779.
- (13) Lee, E.; Kundu, A.; Jeon, J.; Cho, M. Water Hydrogen-Bonding Structure and Dynamics near Lipid Multibilayer Surface: Molecular Dynamics Simulation Study with Direct Experimental Comparison. *J. Chem. Phys.* **2019**, *151* (11), No. 114705.
- (14) von Hansen, Y.; Gekle, S.; Netz, R. R. Anomalous Anisotropic Diffusion Dynamics of Hydrated Water at Lipid Membranes. *Phys. Rev. Lett.* **2013**, *111* (11), No. 118103.
- (15) Martelli, F.; Crain, J.; Franzese, G. Network Topology in Water Nanoconfined between Phospholipid Membranes. *ACS Nano* **2020**, *14* (7), 8616–8623.
- (16) Höglberg, C.-J.; Lyubartsev, A. P. A Molecular Dynamics Investigation of the Influence of Hydration and Temperature on Structural and Dynamical Properties of a Dimyristoylphosphatidylcholine Bilayer. *J. Phys. Chem. B* **2006**, *110* (29), 14326–14336.
- (17) Yamamoto, E.; Akimoto, T.; Hirano, Y.; Yasui, M.; Yasuoka, K. Power-Law Trapping of Water Molecules on the Lipid-Membrane Surface Induces Water Retardation. *Phys. Rev. E* **2013**, *87* (5), No. 052715.
- (18) Hansen, F. Y.; Peters, G. H.; Taub, H.; Miskowiec, A. Diffusion of Water and Selected Atoms in DMPC Lipid Bilayer Membranes. *J. Chem. Phys.* **2012**, *137* (20), No. 204910.
- (19) Martelli, F.; Ko, H.-Y.; Borallo, C. C.; Franzese, G. Structural Properties of Water Confined by Phospholipid Membranes. *Front. Phys.* **2018**, *13* (1), No. 136801.
- (20) Malik, S.; Debnath, A. Dehydration Induced Dynamical Heterogeneity and Ordering Mechanism of Lipid Bilayers. *J. Chem. Phys.* **2021**, *154* (17), No. 174904.
- (21) Calero, C.; Stanley, H.; Franzese, G. Structural Interpretation of the Large Slowdown of Water Dynamics at Stacked Phospholipid Membranes for Decreasing Hydration Level: All-Atom Molecular Dynamics. *Materials* **2016**, *9* (5), 319.
- (22) Wang, B.; Kuo, J.; Bae, S. C.; Granick, S. When Brownian Diffusion Is Not Gaussian. *Nat. Mater.* **2012**, *11* (6), 481–485.
- (23) Song, S.; Park, S. J.; Kim, M.; Kim, J. S.; Sung, B. J.; Lee, S.; Kim, J.-H.; Sung, J. Transport Dynamics of Complex Fluids. *Proc. Natl. Acad. Sci. U.S.A.* **2019**, *116* (26), 12733–12742.
- (24) Rahman, A.; Singwi, K. S.; Sjölander, A. Theory of Slow Neutron Scattering by Liquids. *I. Phys. Rev.* **1962**, *126* (3), 986–996.
- (25) Rahman, A. Correlations in the Motion of Atoms in Liquid Argon. *Phys. Rev.* **1964**, *136* (2A), A405–A411.
- (26) Dickson, C. J.; Madej, B. D.; Skjevik, Å. A.; Betz, R. M.; Teigen, K.; Gould, I. R.; Walker, R. C. Lipid14: The Amber Lipid Force Field. *J. Chem. Theory Comput.* **2014**, *10* (2), 865–879.
- (27) Odagaki, T.; Hiwatari, Y. Gaussian-to-Non-Gaussian Transition in Supercooled Fluids. *Phys. Rev. A* **1991**, *43* (2), 1103–1106.
- (28) Wagner, W.; Prüß, A. The IAPWS Formulation 1995 for the Thermodynamic Properties of Ordinary Water Substance for General and Scientific Use. *J. Phys. Chem. Ref. Data* **2002**, *31* (2), 387–535.
- (29) Szabo, A.; Schulten, K.; Schulten, Z. First Passage Time Approach to Diffusion Controlled Reactions. *J. Chem. Phys.* **1980**, *72* (8), 4350–4357.